Stereospecific Interaction of a Novel Spirosuccinimide Type Aldose Reductase Inhibitor, AS-3201, with Aldose Reductase

Masuo Kurono,* Iwao Fujiwara, and Koji Yoshida

Discovery Research Laboratories, Dainippon Pharmaceutical Company, Ltd., Enoki 33-94, Suita, Osaka 564-0053, Japan

Received February 8, 2001; Revised Manuscript Received May 7, 2001

ABSTRACT: Aldose reductase (AR) is an NADPH-dependent enzyme implicated in diabetic complications. AS-3201 [(*R*)-(−)-2-(4-bromo-2-fluorobenzyl)-1,2,3,4-tetrahydropyrrolo[1,2-*a*]pyrazine-4-spiro-3′-pyrrolidine-1,2′,3,5′-tetrone] is a structurally novel and potent ARI with an inhibitor constant ($K_i = 10^{-10}$ M) 2000-fold lower than that of its optical antipode (*S*-isomer). To elucidate the inhibition modes and the stereochemical differences in their inhibitory potencies, we examined the interaction of these *R*- and *S*-isomers with AR under physiological conditions. Enzyme kinetic analysis, which was performed by using physiological substrates at 37 °C, showed that both isomers selectively act on the E−NADP$^+$ complex in both the forward and reverse reactions of AR. However, fluorometric titration analysis demonstrated that the affinities of the isomers for the E−NADP$^+$ complex are about the same as those for the E−NADPH complex and the apoenzyme. These results suggested that the selective binding to the E−NADP$^+$ complex arises from the predominance of this enzyme form during steady-state turnover rather than from binding specificity. Both the competition with a known active site-directed ARI and the protective effect on AR inactivation by *N*-bromosuccinimide showed that the isomers bind to the active site of the enzyme, but the thermodynamic parameters for the binding to AR indicated that additional hydrogen bonds and/or van der Waals interactions contribute to the energetic stabilization in the E−*R*-isomer complex. Molecular modeling, together with the deductions from spectroscopic studies, suggested that the succinimide ring and the 4-bromo-2-fluorobenzyl group of the *R*-isomer are optimally located for formation of a hydrogen-bonding network with AR, and that the latter benzyl group is also effective for the differentiation between AR and aldehyde reductase (a closely related enzyme).

Aldose reductase (AR,[1] EC 1.1.1.21), a member of the aldo-keto reductase superfamily, is a monomeric and NADPH-dependent enzyme that catalyzes the reduction of aldo sugars and a variety of aldehydes to their corresponding alcohols. AR is a rate-limiting enzyme in the "polyol pathway", where D-glucose is converted to fructose via D-sorbitol (*1*, *2*). The enhancement of this pathway in diabetes is assumed to cause intracellular accumulation of D-sorbitol due to the low permeability across the cell membrane; this brings about secondary diabetic complications such as neuropathy, nephropathy, retinopathy, and cataract (*3*, *4*). Another speculative consequence of increased AR activity is a competition with nitric oxide (NO) synthetase for NADPH to repress NO production in tissues. This decrease in the NO level would lead to a decrease in nerve blood flow and, consequently, to nerve ischemia and diabetic neuropathy (*5*). Therefore, a control of the polyol pathway activation in hyperglycemia is necessary to prevent secondary diabetic complications.

Although several classes of AR inhibitors (ARIs) have been discovered and clinically evaluated, discordant results have been reported in clinical trials on both the effect of ARIs and the prevention of early lesions associated with diabetic complications (*6*, *7*). One reason for the undesirable results can be attributed to the incomplete and nonselective enzyme inhibition of ARIs (*8*, *9*), although some of the clinical trial designs may have been unsatisfactory (*10*). To design a new class of ARIs with more potent and fewer adverse effects, the kinetic properties and the active site catalytic residue(s) of AR have been examined in detail. AR follows an ordered bi-bi mechanism where NADPH binds to the enzyme first prior to the binding of aldehyde substrates and then NADP$^+$ is released last after the liberation of the alcohol products (*11*−*13*). In this reaction sequence, conformational changes just before the NADP$^+$ release are the rate-determining step, and Tyr48 is most likely the active site catalytic residue (*14*, *15*). In parallel, it is of importance to gain insights into the interaction of structurally diverse ARIs with the enzyme. However, the interaction of ARIs with AR has been less well characterized except for carboxylic acid type and spirohydantoin type ARIs.

* To whom correspondence should be addressed. Phone: +81-6-6337-5886. Fax: +81-6-338-7656. E-mail: masuo-kurono@dainippon-pharm.co.jp.

[1] Abbreviations: AR, aldose reductase; ALR, aldehyde reductase; ARI, aldose reductase inhibitor; NADPH and NADP$^+$, nicotinamide adenine dinucleotide phosphate, reduced and oxidized forms, respectively; NBS, *N*-bromosuccinimide; bis-trispropane (BTP), 1,3-bis[tris(hydroxymethyl)methylamino]propane; AS-3201 (*R*-isomer), (*R*)-(−)-2-(4-bromo-2-fluorobenzyl)-1,2,3,4-tetrahydropyrrolo[1,2-*a*]pyrazine-4-spiro-3′-pyrrolidine-1,2′,3,5′-tetrone; SX-3202 (*S*-isomer), (*S*)-(+)-2-(4-bromo-2-fluorobenzyl)-1,2,3,4-tetrahydropyrrolo[1,2-*a*]pyrazine-4-spiro-3′-pyrrolidine-1,2′,3,5′-tetrone; SX-3212 (racemate), 2-[2-(4-bromo-2-fluorobenzyl)-1,2,3,4-tetrahydro-1,3-dioxopyrrolo[1,2-*a*]pyrazin-4-yl]acetamide; ponalrestat, 3-[(4-bromo-2-fluorophenyl)methyl]-3,4-dihydro-4-oxo-1-phthalazineacetic acid; zopolrestat, 3,4-dihydro-4-oxo-3-{[5-(trifluoromethyl)-2-benzothiazolyl]methyl}-1-phthalazineacetic acid.

10.1021/bi0102813 CCC: $20.00 © 2001 American Chemical Society
Published on Web 06/22/2001

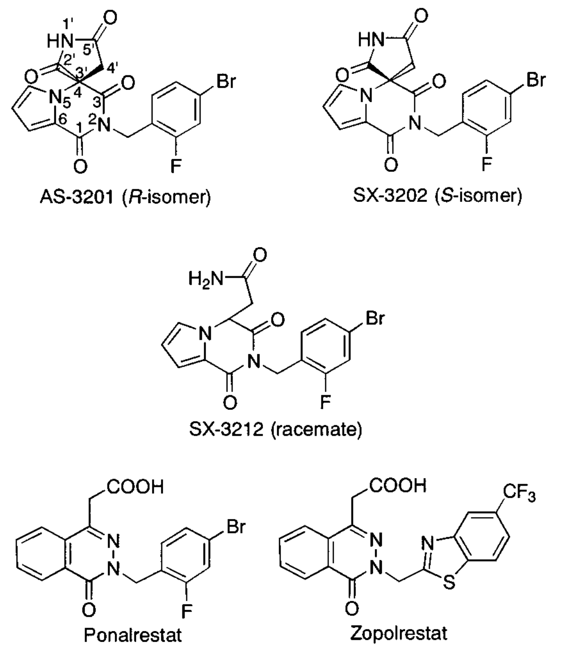

FIGURE 1: Chemical structures of ARIs used in this study. The asymmetric carbon that determines the *R*- or *S*-configuration is C4 (C3′) of the molecule.

AS-3201 [(*R*)-(−)-2-(4-bromo-2-fluorobenzyl)-1,2,3,4-tetrahydropyrrolo[1,2-*a*]pyrazine-4-spiro-3′-pyrrolidine-1,2′,3,5′-tetrone (Figure 1)] is a structurally novel and stereospecifically potent ARI with improved pharmacokinetics (*16*). This compound is more potent in both the AR inhibition and in vivo activity than its optical antipode (*S*-isomer, SX-3202, Figure 1) and is expected to be a clinical candidate for the treatment of diabetic complications. To gain a better understanding of the stereospecificity in enzyme inhibition, we investigated the interaction between AS-3201 (*R*-isomer) and AR under physiological conditions (37 °C and physiological substrates, D-glucose and D-sorbitol). The use of the *S*-isomer enabled us to perform comparative studies of the interactions of the present enzyme−inhibitor (E−I) complexes. We discussed the observed inhibition kinetics in terms of the mechanism of the AR reaction (*12*, *13*, *15*), and characterized the binding of the isomers to AR by performing spectroscopic and molecular modeling studies. These data should provide our spirosuccinimide type inhibitors with more plausible binding modes that could describe the stereospecific and selective interaction in the binding site.

MATERIALS AND METHODS

Materials. Recombinant human AR, produced in *Spodoptera frugiperda* cells (*17*), was purchased from Wako Pure Chemical Industries, Ltd. (Osaka, Japan). *N*-Bromosuccinimide (NBS) was from Aldrich and recrystallized from water before use. All other chemicals were of the highest purity available. AS-3201 (*R*-isomer, optical purity of ≥99.8% ee), SX-3202 (*S*-isomer, optical purity of ≥99.8% ee), SX-3212 (racemate), and ponalrestat (Figure 1) were synthesized in our laboratories (*16*). Ponalrestat was used as a reference compound; this compound bears in part a common structure with zopolrestat (Figure 1), and it resembles zopolrestat with respect to the mode of binding to the active site pocket of AR (*18*, *19*). The compounds were dissolved in acetonitrile, and these stock solutions (5−10 mM) were diluted with a mixture of 1 mM citric acid (pH 2.8) and acetonitrile (90:10, v/v) to the desired concentrations before being used. We checked that this diluent had no influence on the enzyme activity because of the low concentrations of the additives (0.4% acetonitrile and 0.03 mM citric acid) under the experimental conditions. Bis-trispropane (BTP)-HCl buffers (50 mM, pH 5.3−8.1, ionic strength of 0.5−0.14) were used for kinetic and binding studies unless otherwise stated, and their pHs were measured at the temperature at which the experiment was carried out. Distilled and deionized (<0.1 μS/cm) water was used for all the measurements.

Steady-State Kinetic Studies. In 50 mM BTP-HCl buffer (pH 7.7), standard reaction mixtures (3 mL) contained the enzyme (typically 13 nM), 150 μM NADPH (coenzyme), 150 mM D-glucose (substrate), and 150 μL of the diluent (see Materials) with or without inhibitors. The reaction was initiated by adding D-glucose to the reaction mixture at 37 °C, and enzyme activity (initial velocity) was measured on a HITACHI U-3210 spectrophotometer (Hitachi Ltd., Tokyo, Japan) through the decrease in NADPH absorbance at 340 nm. Kinetic constants were determined by fitting the activities at various D-glucose concentrations to either the Michaelis−Menten equation or the general equation for substrate inhibition (*20*). Reaction mixtures free of the enzyme or the substrate were used as the controls. For the reverse reaction, NADPH and D-glucose were replaced with $NADP^+$ and D-sorbitol, respectively, and the increase in absorbance at 340 nm due to NADPH formation was followed.

The apparent inhibitor constant (K_i') was obtained by measuring the residual activity as a function of the inhibitor concentration in the presence of a saturating concentration (150 μM) of coenzyme and a fixed nonsaturating concentration of substrate. During inhibition by the *S*-isomer, the enzyme activity significantly decreased only when the *S*-isomer concentration was much greater than the enzyme concentration. This assumes that the concentration of the free *S*-isomer (I_f) approximates the total concentration of the *S*-isomer (I) (i.e., classical inhibition). The data were fitted to eq 1 (*21*−*23*)

$$v_i/v_0 = 1/(1 + I/K_i') \tag{1}$$

where v_i/v_0 is the residual activity (v_i and v_0 are the activities in the presence and absence of the inhibitor, respectively). On the other hand, the *R*-isomer is effective at concentrations similar to that of the enzyme. This finding means that a significant fraction of the *R*-isomer is bound to the enzyme and that the approximation ($I_f = I$) becomes inaccurate (i.e., tight-binding inhibition). Under such circumstances, allowance must be made for the reduction in the concentration of the free *R*-isomer, and the data were fitted to eq 2, which accounts for depletion of the free inhibitor (*24*, *25*)

$$v_i/v_0 = [E - I - K_i' + \sqrt{(E - I - K_i')^2 + 4EK_i'}]/(2E) \tag{2}$$

where E is the enzyme concentration. If the value of I is much greater than E ($I \gg E$), eq 2 becomes identical to eq 1. Thus, eq 2 can also describe classical inhibition, but eq 2 should not be applied in this case because inclusion of an extra parameter (E) may increase the uncertainty in the determination of K_i'.

To decide inhibition type, the slope (competitive) and the intercept (uncompetitive) inhibitor constants, K_{is} and K_{ii} (*26*), respectively, were calculated by fitting the K_i' values obtained at different substrate concentrations to eq 3 for general mixed noncompetitive inhibition (*21*, *27*)

$$K_i' = K_{is}K_{ii}(K_m + A)/(K_{is}A + K_mK_{ii}) \quad (3)$$

where A is the substrate concentration and K_m is the Michaelis constant of A. The plot of K_i' versus A will be concave-up when $K_{is} > K_{ii}$ and concave-down when $K_{is} < K_{ii}$. When A tends to zero, K_i' will equal K_{is}, whereas when A tends to infinity, K_i' will equal K_{ii} (*24*, *27*). Comparison of K_{is} with K_{ii} revealed the inhibition to be competitive ($10K_{is} \leq K_{ii}$), uncompetitive ($K_{is} \geq 10K_{ii}$), or mixed ($K_{is} \approx K_{ii}$).

Steady-State Fluorescence Measurements. Dissociation constants were determined from the quenching of protein fluorescence on a Shimadzu RF-5300 spectrofluorophotometer (excitation and emission bandwidths, 10 or 5 nm) at 37 °C. Titrations were carried out by serial addition of aliquots (3−7 μL) of ligand solutions to 3 mL of enzyme solution (20−50 nM) in 50 mM BTP-HCl (pH 7.2) containing 0.2 mM dithiothreitol. The fluorescence intensities at 340 nm (excitation at 280 nm) were recorded at 2 min after the addition of ligand, and corrected for background Raman scattering and dilution effects. The dependence of fluorescence intensity on ligand concentration was then fitted as previously described to obtain the dissociation constant (K_d) (*28*). To minimize inner filter effects, the sum of the absorbances at both the excitation and emission wavelengths was kept at <0.1.

Cooperative binding to the enzyme was examined by using the postulated general equilibrium model as shown in Scheme 1. K_{dA} and K_{dB} are the dissociation constants of ligands A and B, respectively. K_{dAB} is the dissociation constant for dissociation of ligand A from the E−B (the enzyme fully presaturated with ligand B) complex. Under the present conditions, K_{dAB} is difficult to determine directly because the E−B complex is not experimentally accessible. To obtain K_{dAB}, therefore, the apparent dissociation constant of ligand A (K_{dA}') was measured at different and nonsaturating concentrations of ligand B (B), and the obtained K_{dA}' values were fitted to eq 4 with the value of the dissociation constant for the binary E−B complex (K_{dB}), as described by Birdsall et al.[2] (*29*)

$$K_{dA}' = K_{dA}K_{dAB}(B + K_{dB})/(K_{dA}B + K_{dAB}K_{dB}) \quad (4)$$

Enzyme Concentration. The concentration of AR was determined by titrating the enzyme with the *R*-isomer and by monitoring the decrease in the enzyme activity or the enzyme fluorescence. Identical results were obtained by both the inhibition and fluorescence techniques.

Inactivation of AR by NBS. The enzyme (1 μM) was dissolved in 50 mM BTP-HCl (pH 7.0) containing $NADP^+$ and/or the inhibitor, and the mixture was incubated with NBS (0.4 mM) in the dark at 25 °C for 10 min. The reaction was terminated by diluting the sample 270-fold with the same buffer containing 0.08% human serum albumin (HSA) in addition to 150 μM NADPH and 200 mM D-glucose. HSA was added to quench the unreacted NBS and to trap the inhibitor released from the E−I complex. Then, the enzyme activity of the resulting solution was assayed for evaluation of irreversible AR inactivation by the NBS treatment.

Scheme 1: Equilibria Describing the Binding of Ligands A and B to AR[a]

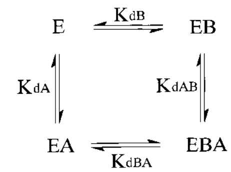

[a] A, AS-3201 (*R*-isomer) or SX-3202 (*S*-isomer); B, $NADP^+$, NADPH, or ponalrestat; E, enzyme.

Fitting of Kinetic Data. Each parameter was calculated by fitting the experimental data to each equation in the text using the Marquardt−Levenberg algorithm in Origin 5.0 (MicroCal Software, Northampton, MA). Weighting was not applied to individual data, and curves were calculated from the fits of the data to an appropriate equation. In the refitting of the calculated values to eqs 3 and 4, however, the reciprocal of the squared standard error was applied as weighting.

^{19}F NMR Spectral Measurements. ^{19}F NMR spectra were obtained at 470 MHz on a Varian Unity-INOVA 500 spectrometer (Varian Associates, Palo Alto, CA) equipped with a 5 mm ^{1}H/^{19}F probe. Measurements were performed without proton decoupling. Standard un-decoupled spectral parameters were as follows: 34 kHz spectral width, 13K data points, 90° (14.5 μs) pulse width, 1.95 s acquisition time, 2.05 s relaxation delay, and temperature control at 25 °C. Fluorine chemical shifts were measured with respect to $CFCl_3$, by using the CF_3 resonance of trifluoroethanol as a secondary reference (−77.23 ppm). Samples contained the enzyme (110 μM), 1% glycerol, 1 mM dithiothreitol, and 1% acetonitrile with or without the isomers. These were dissolved in $^1/_{15}$ M phosphate buffer (pH 7.4).

Molecular Modeling. The initial atomic coordinates of the isomers were referenced to the single-crystal X-ray analysis data (*16*). The geometry was optimized by AM1 in MOPAC 6.0, and the final atomic point charges were obtained by single-point MNDO for the optimized structure.

The structure of AR was reconstituted by using crystal coordinates of the human holoenzyme−zopolrestat complex (1MAR) (*19*). The coordinates include zopolrestat, NADPH, and the C_α atoms of AR. The side chain and the backbone atoms were then added on the basis of the human holoenzyme structure (1ADS) (*30*) with the Biopolymer module supplied by Sybyl 6.3 (Tripos Associates, Inc., St. Louis, MO). The charges were generated by the Kollman all-atom (*31*) for the enzyme and by single-point MNDO for zopolrestat, and the cell multipole method (*32*) was adopted for the evaluation of nonbonded interactions. Conjugate gradient minimization was then performed with Discover 3.0.0 (Molecular Simulations, Inc., San Diego, CA), using the consistent valence force field (*33*). During the calculation, zopolrestat, NADPH, and the C_α atoms of AR were kept fixed in their original positions. The energy minimization

[2] They used the binding constant to refer to the equilibrium, while we used the dissociation constant in this work.

Table 1: Apparent Kinetic Constants for AR-Catalyzed Reduction and Oxidation of D-Glucose and D-Sorbitol, Respectively[a]

substrate	K_m (mM)	k_{cat} (s^{-1})	k_{cat}/K_m (s^{-1} M^{-1})
D-glucose	46 ± 3	0.80 ± 0.03	18 ± 1
D-sorbitol	760 ± 150	0.66 ± 0.10	0.88 ± 0.05

[a] The activity was assayed with 150 μM NADPH or $NADP^+$ in 50 mM BTP-HCl (pH 7.7) at 37 °C. Except where noted, the errors are the calculated standard errors of the fit.

of the system was broken up within 1000 iterations before reaching the maximum derivative of 0.1 kcal mol^{-1} $Å^{-1}$, and the resulting structure was used as the starting point for the docking study.

For the docking and molecular mechanics calculations, the succinimide ring of the *R*-isomer (or the *S*-isomer) was taken as dissociated, and docked into the active site, allowing one of the oxygen atoms of the succinimide ring to interact with Tyr48 OηH. Then, the carbonyl oxygen at C3 of its pyrrolopyrazine framework was allowed to interact with Cys298 SγH. The 4-bromo-2-fluorobenzyl group (the pendent benzyl group) was positioned between Trp111 and Leu300 such that the 4-bromine atom pointed to Thr113 Oγ1H. Flexible docking was performed with FlexiDock implemented in Sybyl, which employs a genetic algorithm for energy-based optimization. The evaluation function was based on the Tripos force field (*34*), and the bond stretching, angle bending, and out-of-plane bending terms were invariant in torsional space optimization and, therefore, ignored. The optimization by FlexiDock was examined on the restrained E−I complex in which the translation and the torsional angles of the isomer(s) and the side chains of proximal amino acids (Trp20, Tyr48, His110, Trp111, Thr113, Phe122, and Cys298) were left free to move.

RESULTS

Inhibition of AR by the R- and S-Isomers. To clarify AR inhibition by the isomers under physiological conditions, we conducted kinetic studies principally at 37 °C by using physiological substrates, D-glucose and D-sorbitol. Table 1 gives the apparent kinetic constants for D-glucose reduction with NADPH and D-sorbitol oxidation with $NADP^+$ by AR measured at pH 7.7 in the absence of inhibitors. The catalytic efficiency (k_{cat}/K_m) suggested that the enzyme favors the forward reaction (D-glucose reduction). Figure 2A shows the relationship between the residual enzyme activity (v_i/v_0) and the *R*-isomer concentration in the forward reaction with 150 mM D-glucose. A substantial decrease in the activity was observed at isomer concentrations comparable to that of the enzyme (i.e., tight-binding inhibition), and the K_i' value was determined to be 0.45 ± 0.04 nM by fitting the experimental data to eq 2. Figure 2B is a replot of K_i' versus D-glucose concentration. This replot was concave-up, and the data were analyzed by fitting to eq 3 as described in Materials and Methods. In this case, K_{is} was redundant (i.e., $K_{is} \gg K_{ii}$), and the finite value of K_{ii} was determined to be 0.38 ± 0.03 nM. Therefore, the inhibition type was uncompetitive with respect to D-glucose. Figure 3 shows a replot of K_i' versus D-sorbitol concentration in the reverse reaction. In the reverse reaction, K_{ii} was redundant (i.e., $K_{ii} \gg K_{is}$), and the finite value of K_{is} was determined to be 0.32 ± 0.02 nM. Therefore, the inhibition type was competitive with respect to D-sorbitol.

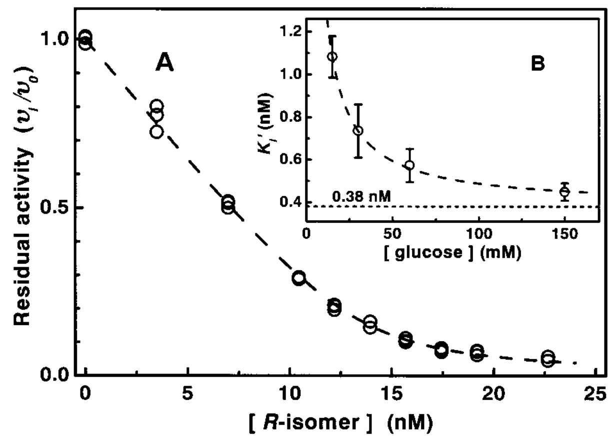

FIGURE 2: (A) Inhibition of AR by the *R*-isomer in the forward reaction with 150 mM D-glucose at pH 7.7 and 37 °C. [AR] = 13.7 nM. The dashed line is the theoretical curve with a K_i' of 0.45 nM. (B) Replot of the evaluated K_i' vs D-glucose concentration. The curve was drawn by using the calculated K_{ii} (K_{is} was redundant), which was determined by fitting to eq 3 together with the K_m for D-glucose.

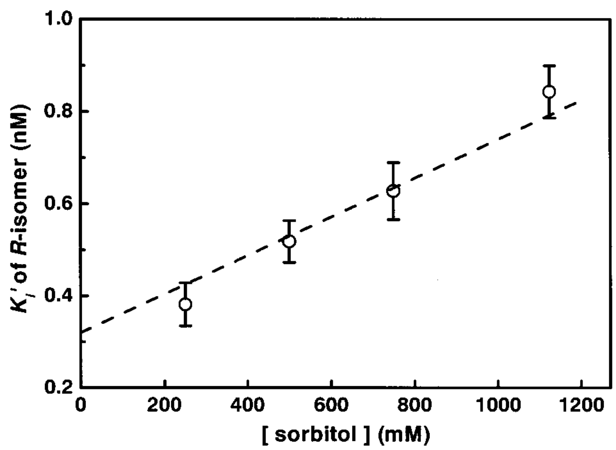

FIGURE 3: Replot of the evaluated K_i' of the *R*-isomer in the reverse reaction vs D-sorbitol concentration. The curve was drawn by using the calculated K_{is} (K_{ii} was redundant), which was obtained by fitting to eq 3 together with the K_m for D-sorbitol.

It has been recognized that an irreversible inhibitor exhibits noncompetitive type inhibition and its K_i' value is independent of the substrate concentration because it decreases the actual initial concentration of the enzyme (*35*, *36*). In the study presented here, a consideration of inhibition patterns described above clearly indicated that the *R*-isomer reversibly binds to the enzyme, and its binding attains equilibrium fairly rapidly under the present conditions (37 °C, pH 7.7, D-glucose or D-sorbitol as the substrate). The *S*-isomer also followed uncompetitive kinetics against D-glucose in the forward reaction and competitive kinetics against D-sorbitol in the reverse reaction (data not shown); however, the evaluated K_{ii} and K_{is} values were, respectively, more than 2000-fold greater than those for the *R*-isomer. These results are summarized in Table 2. In contrast, the succinimide ring-opening compound (SX-3212, Figure 1) had no inhibitory activity, which strongly shows that the succinimide ring in the pyrrolopyrazine framework is essential for the formation of the E−I complex.

pH and Temperature Dependence of Inhibition. We examined the pH dependence of K_{ii} in the pH range of 5.3−8.1. Ponalrestat, an active site-directed ARI (*18*), displayed

Table 2: Inhibitor Constants Obtained for AR-Catalyzed Reduction and Oxidation of D-Glucose and D-Sorbitol, Respectively[a]

	forward		reverse	
	pattern	K_i[b] (nM)	pattern	K_i[b] (nM)
AS-3201 (*R*-isomer)	UC	0.38 ± 0.03	C	0.32 ± 0.02
SX-3202 (*S*-isomer)	UC	870 ± 10	C	650 ± 10

[a] The activity was assayed with 150 μM NADPH or $NADP^+$ in 50 mM BTP-HCl (pH 7.7) at 37 °C. [b] K_i values represent K_{is} and K_{ii} for competitive (C) and uncompetitive (UC) inhibition, respectively.

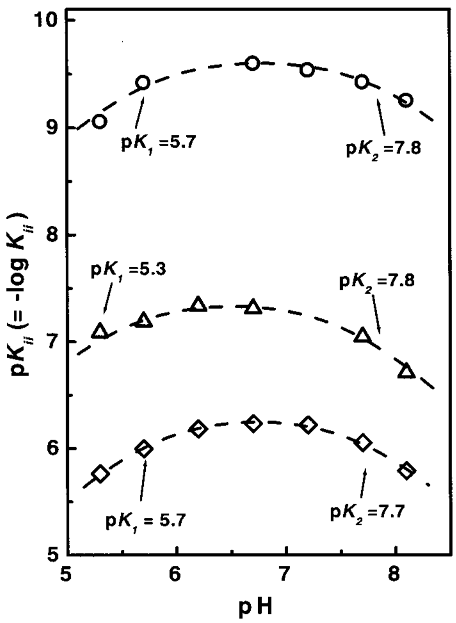

FIGURE 4: pK_{ii}−pH profiles of the *R*-isomer (○), the *S*-isomer (◇), and ponalrestat (△) in the forward reaction of AR. The curves and p*K* values that are shown were calculated by fitting the data to eq 5.

uncompetitive inhibition in the forward reaction with a K_{ii} value of 10^{-8} M, a value similar to that reported by Bhatnagar et al. (*37*). As shown in Figure 4, the pK_{ii}−pH profiles for the isomers and ponalrestat yielded bell-shaped curves, and two apparent p*K* (pK_1 and pK_2) values were obtained by fitting the data to eq 5.

$$-\log K_{ii} = \log[K_{ii(max)}/(1 + [H]/K_1 + K_2/[H])] \quad (5)$$

where K_1 and K_2 are the dissociation constants of the ionizable groups that affect E−I complex formation. The evaluated pK_1 values on the acidic side for ponalrestat (p$K \le 5.3$) and the isomers (p$K = 5.7$) may be attributable to the carboxylate (*38*) and the succinimide,[3] respectively. It appears that the deprotonation of these inhibitors plays an important role in binding to AR. On the other hand, the pK_2 value on the basic side (p$K = 7.7-7.8$) should be assigned to an ionizable group in the enzyme. Protonation or deprotonation of this group or the groups surrounding this ionizable group in the enzyme could modulate the interactions with these inhibitors. Thus, the binding of our isomers to the enzyme had a feature in common with that of ponalrestat.

To examine the energetics of formation of the complexes, we determined thermodynamic parameters for the binding

[3] Both a potentiometric titration and a spectrophotometric determination have shown that the isomers possess a p*K* of 5.6−5.7 under similar conditions (unpublished data).

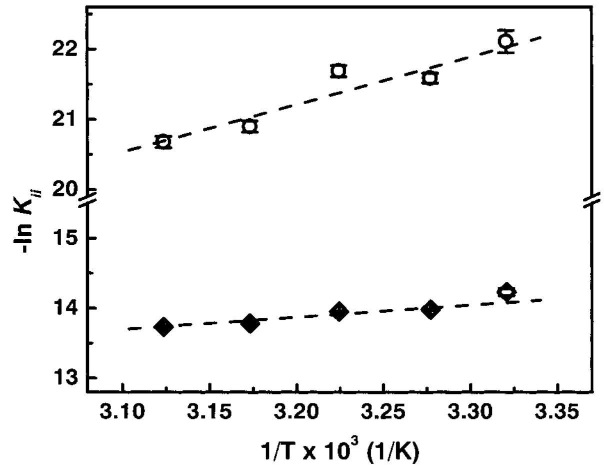

FIGURE 5: Temperature dependence of the K_{ii} values (van't Hoff plot) of the *R*-isomer (○) and the *S*-isomer (◇) at pH 7.7.

Table 3: Thermodynamic Parameters for the Binding of the Isomers to AR at 37 °C and pH 7.7[a]

inhibitor	$\Delta G°$ (kJ mol^{-1})	$\Delta H°$ (kJ mol^{-1})	$\Delta S°$ (J mol^{-1} $°C^{-1}$)
AS-3201 (*R*-isomer)	-56 ± 1	-56 ± 5	-4 ± 16
SX-3202 (*S*-isomer)	-36 ± 1	-14 ± 1	69 ± 3

[a] $\Delta G°$ was calculated from the K_{ii} values, $\Delta H°$ from the slope of the linear van't Hoff plot, and $\Delta S°$ from the relationship $\Delta S° = (\Delta H° - \Delta G°)/T$.

of the *R*- and *S*-isomers to AR. Figure 5 shows the temperature dependence of K_{ii} exemplified by the van't Hoff plots (−ln K_{ii} vs 1/*T*). The van't Hoff plots were essentially linear in the range of 27−47 °C[4] at pH 7.7, and their slopes were positive for both isomers, whose affinities decreased with the increase in temperature. The calculated thermodynamic quantities, namely, the standard Gibbs energy change ($\Delta G°$), the enthalpy change ($\Delta H°$), and the standard entropy change ($\Delta S°$), are listed in Table 3. As would be predicted from the deprotonation of the succinimide ring (see above), the formation of the complexes was driven by favorable negative ΔH, but there was a wide difference between these two values. In addition, their complex formations were differentiated by a significant difference in the entropy changes. As a whole, the binding of the *S*-isomer was both enthalpically and entropically driven, whereas that of the *R*-isomer was essentially enthalpically driven.

Fluorometric Titration of AR with the Isomers and Other Ligands. Figure 6 shows the fluorescence spectra of AR in the presence or absence of the *R*- and *S*-isomers, upon excitation at 280 nm. The fluorescence intensity at ~340 nm was largely decreased by the addition of the isomers, clearly indicating that the isomers bind to the apoenzyme (ligand free enzyme), and that the fluorescent Trp or Tyr residues are located at or near the binding site of the isomers. The *R*-isomer induced a 4 nm blue shift in the emission maximum while the *S*-isomer a 2 nm shift, suggesting that the E−*R*-isomer and E−*S*-isomer complexes differ from each

[4] Although the apoenzyme (ligand free enzyme) was gradually inactivated at 47 °C, this thermal inactivation was definitely prevented in the presence of a saturating concentration of coenzyme (NADPH or $NADP^+$) under the present conditions. The enzyme retained catalytic activity at 47 °C for all observation periods (at least up to 20 min).

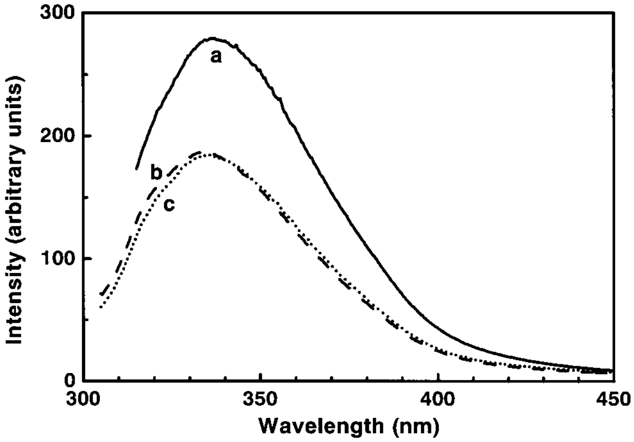

FIGURE 6: Fluorescence spectra of AR and its complexes with the *R*- and *S*-isomers (excitation at 280 nm). The enzyme concentration is 0.21 μM. The spectra were measured before (a) and after addition of 0.19 μM *R*-isomer (b) and 7.7 μM *S*-isomer (c).

Table 4: Dissociation Constants (K_d) of Various AR−Ligand Complexes[a]

ligand	enzyme form	K_d (nM)
AS-3201 (*R*-isomer)	E	0.79 ± 0.11
	E−NADPH	0.6 ± 0.1
	E−NADP$^+$	0.5 ± 0.1
	E−ponalrestat	infinity
SX-3202 (*S*-isomer)	E	(1.2 ± 0.1) × 10^3
	E−NADPH	(8.0 ± 0.3) × 10^2
	E−NADP$^+$	(8.4 ± 0.2) × 10^2
ponalrestat	E	57 ± 1
NADPH	E	240 ± 10
NADP$^+$	E	170 ± 10

[a] Dissociation constants were determined by fluorescence titration in 50 mM BTP-HCl buffer (pH 7.2) with 0.2 mM dithiothreitol at 37 °C.

other in the local environment around these fluorescent residues.[5] Dissociation constants of the isomers (K_d) were determined from the dependence of the fluorescence decrease upon ligand concentration. The results are summarized in Table 4. The apoenzyme essentially differentiates the *R*-isomer from the *S*-isomer. The K_d values of ponalrestat and coenzymes (NADPH and NADP$^+$) were also determined (Table 4); those of coenzymes are similar to those previously reported for human AR (*39*, *40*).

To investigate the cooperative interaction between the isomers and another ligand, the alteration in the K_d values of the isomers was examined in the presence of coenzymes or ponalrestat (see Materials and Methods). Typical plots of the apparent dissociation constant (K_{dA}') versus the NADP$^+$ concentration are illustrated in Figure 7. The K_{dA}' values of the isomers gradually decreased as the concentration of NADP$^+$ increased. The dissociation constant for dissociation of the *R*-isomer (or the *S*-isomer) from the E−NADP$^+$ complex[6] (K_{dAB}) was determined to be 0.5 ± 0.1 (or 840 ± 20) nM by fitting the data to eq 4. Also, the K_{dA}' values of the isomers decreased with the addition of NADPH (data

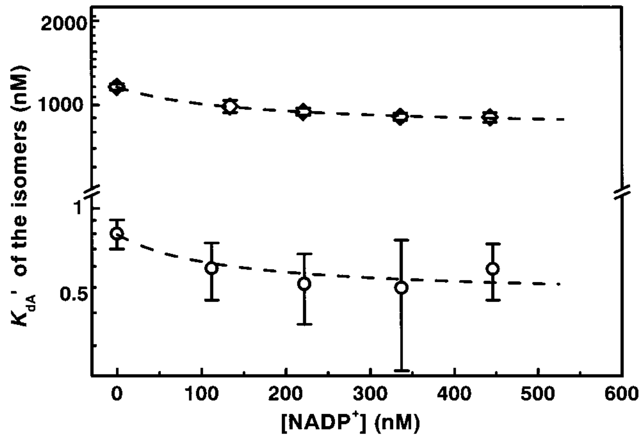

FIGURE 7: Replots of the logarithm of the apparent dissociation constants, K_{dA}', of the *R*-isomer (○) and the *S*-isomer (◇) vs NADP$^+$ concentration. The curves were drawn by using the calculated K_{dAB} and the experimentally obtained K_{dB}.

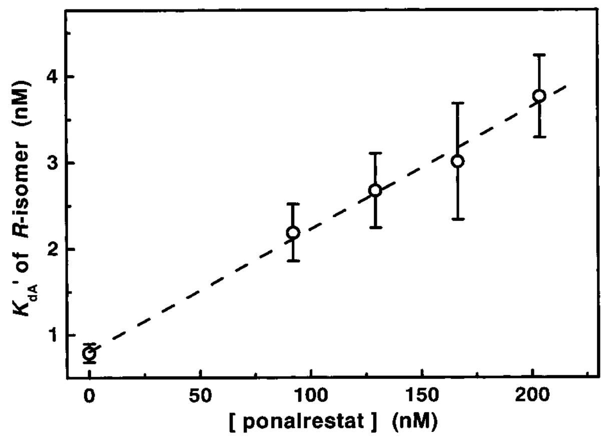

FIGURE 8: Replot of the K_{dA}' of the *R*-isomer vs ponalrestat concentration. The data were obtained by using the same procedures as described in the legend of Figure 7.

not shown), and the estimated dissociation constant for dissociation of the *R*-isomer (or the *S*-isomer) from the E−NADPH complex (K_{dAB}) was almost the same as that for the E−NADP$^+$ complex (Table 4). These results show that NADPH facilitates the binding to the same extent, as does NADP$^+$. In contrast, the binding of the *R*-isomer to the enzyme seems to be inhibited by ponalrestat.[7] As shown in Figure 8, K_{dA}' of the *R*-isomer[8] increased linearly with the concentration of ponalrestat. The estimated K_{dAB} value between the *R*-isomer and the E−ponalrestat complex approached infinity, and this indicates that the *R*-isomer and ponalrestat are mutually exclusive to the enzyme.

Effect of Inhibitor Binding on AR Inactivation by NBS. The level of inactivation of the enzyme was proportional to the amount of NBS that was used, and the remaining activity

[5] We checked that the same spectra were observed on excitation at 295 nm, where Tyr scarcely absorbs, showing that Trp was selectively excited due to the energy transfer from Tyr to Trp residues.

[6] The E−NADP$^+$ complex is used to denote the NADP$^+$-bound enzyme irrespective of whether the structural isomerization occurs on NADP$^+$ binding. That goes for the E−NADPH complex as well.

[7] When ponalrestat was used as ligand B, the concentration of ligand B (B) in eq 4 was approximated by $B - E$ (i.e., the total concentration of ponalrestat minus the enzyme concentration), for the ponalrestat concentration was not considerably greater than the enzyme concentration under the present conditions and the formation of the E−ponalrestat complex reduced the concentration of free ponalrestat.

[8] Because of the low affinity for the enzyme, the concentration of the *S*-isomer required for measurements was greater than 1 × 10^{-6} M; this caused serious inner filter effects and made it impossible to accurately investigate the variation in the apparent dissociation constant (K_{dA}').

Table 5: Effects of SX-3202 (*S*-isomer) and Ponalrestat on the Inactivation of AR by NBS[a]

treatment	residual activity (%)
none (control)	100 ± 5
NBS	7.4 ± 3.2
NBS and $NADP^+$	8.5 ± 3.0
NBS and *S*-isomer (47 μM)	62 ± 4
NBS and ponalrestat (2 μM)	52 ± 3
NBS, $NADP^+$, and *S*-isomer (47 μM)	61 ± 2
NBS, $NADP^+$, and ponalrestat (2 μM)	51 ± 9

[a] The enzyme was incubated at pH 7.0 and 25 °C with 0.42 mM NBS in the absence or presence of the ligands. The $NADP^+$ concentration was set to 52 μM. The residual AR activity was calculated from the activity of control AR (treated as described above in the absence of NBS).

of AR (1 μM) was 7% of the initial one after incubation for 10 min with NBS (0.4 mM). NBS reacts readily with exposed Trp residues in proteins, decreasing the absorbance at 280 nm (*41*). However, at high molar ratios with respect to the enzyme, NBS can react with Tyr residue(s) accompanying an increase in absorbance at 280 nm (*42*). In the present reaction, we assumed that Tyr residue(s) is modified because the absorbance at 280 nm increased (data not shown). Ponalrestat, an active site-directed ARI, significantly protected the enzyme from inactivation by NBS, but $NADP^+$ did not resist the attack by NBS (Table 5) even in a situation where the enzyme was wholly saturated with this coenzyme (52 μM). This finding indicated that the residue(s) to be oxidized by NBS is at or near the binding site of ponalrestat (i.e., the active site of the enzyme), but not of the coenzyme. The addition of the *S*-isomer provided significant protection against AR inactivation by NBS,[9] although the concentration required for the protection was much higher than that of ponalrestat. This may reflect the high K_i (or K_d) value of the former compared with that of the latter. No synergistic effect was observed with the inhibitor−$NADP^+$ combinations.

^{19}F NMR Measurements. The ^{19}F NMR measurements were carried out to experimentally obtain information about the local environment of the 4-bromo-2-fluorobenzyl group moiety in the complex. Figure 9 shows the ^{19}F NMR spectra of the *R*- or *S*-isomer in the absence or presence of AR. The ^{19}F signal of the isomers (at −116.01 ppm) obtained in the absence of the enzyme exhibited the splitting pattern due to ^{19}F−^{1}H multiple couplings. The signal for the bound *R*-isomer was observed at −116.80 ppm, which is shifted upfield by 0.79 ppm from the signal of the free isomer, while that for the bound *S*-isomer was shifted substantially downfield. During the titration, the signals of the bound and free *R*-isomer were observed without a significant change in their resonance positions, suggesting that the *R*-isomer binds to the enzyme at a rate slower than the NMR time scale (slow exchange). In contrast, the signals of the bound and free *S*-isomer were observed to approach each other gradually as the *S*-isomer concentration increased (slow to intermediate exchange). Hence, the chemical shift of the bound *S*-isomer was estimated by extrapolation to be approximately −113.0 ppm. When the *R*-isomer was added to the *S*-isomer-bound

[9] Under the present conditions, the binding of the *R*-isomer to the enzyme was so strong that this isomer was not completely liberated from the enzyme even in the presence of human serum albumin as an inhibitor trap.

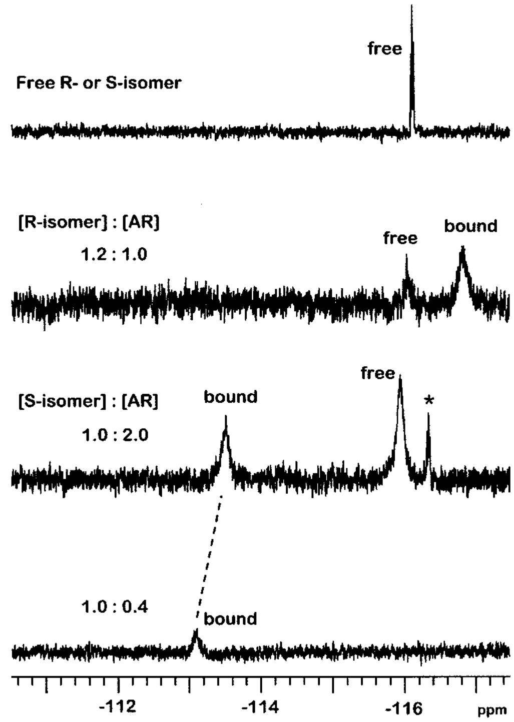

FIGURE 9: ^{19}F NMR spectra of the *R*- or *S*-isomer in either the absence or presence of AR (110 μM). The asterisk marks the signal that arises from SX-3212, which was formed by the hydrolysis of the succinimide ring of the isomer.

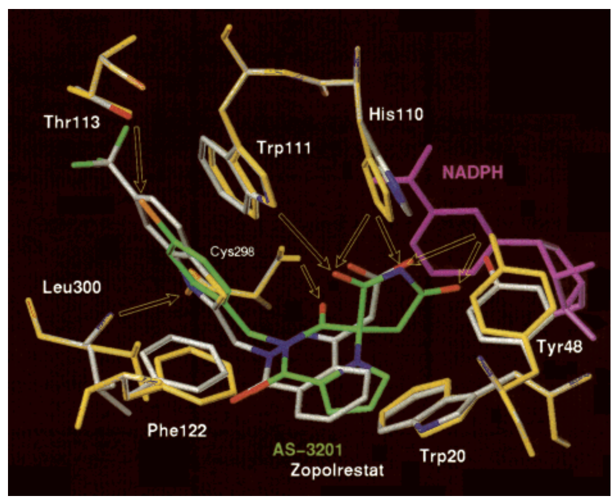

FIGURE 10: Superposed E−I complexes of the energy-minimized zopolrestat (gray) and the flexible docked AS-3201 (*R*-isomer) (green) in the active site of AR. The side chains of proximal residues for the zopolrestat complex are shown in gray and those for the *R*-isomer complex in yellow. The arrows show hydrogen bonds (heteroatom−hydrogen distance of ≤2.9 Å).

AR solution, the signal for the bound *S*-isomer disappeared, followed by the appearance of the signal for the bound *R*-isomer. On the contrary, addition of the *S*-isomer to the *R*-isomer-bound enzyme solution did not cause any spectral alteration. Therefore, the results show that the *R*-isomer binds to the binding site of the *S*-isomer in AR with a binding affinity greater than that of the *S*-isomer.

Modeled Interaction of the Isomers with the Holoenzyme. Figure 10 shows the flexible docked structure of AS-3201 (*R*-isomer) superposed on the reconstituted structure of zopolrestat at the active site of AR (see Materials and Methods). The *R*-isomer fitted nicely into the entire active

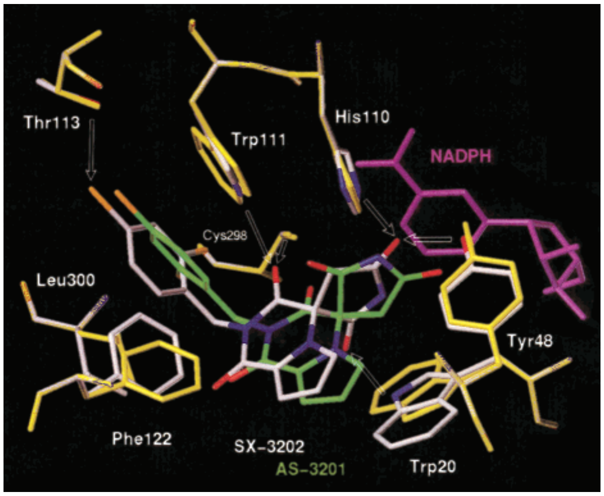

FIGURE 11: Superposed E−I complexes of the flexible docked AS-3201 (*R*-isomer) (green) and SX-3202 (*S*-isomer) (gray) in the active site of AR. Note the changes of the side chains of Trp20, Trp111, and Phe122 (gray) for the *S*-isomer complex, and the relative orientation of the 4-bromo-2-fluorobenzyl group of the *S*-isomer.

site pocket in an orientation similar to that of zopolrestat. The succinimide ring in the pyrrolopyrazine framework was located at the active site, and the rigidity of the spirosuccinimide oriented the three heteroatoms for hydrogen-bonding interactions with Tyr48 OηH, His110 Nϵ2H, and Trp111 Nϵ1H. This binding model has an orientation similar to that of the spirohydantoin ring observed for sorbinil and fidarestat (*43*, *44*). On the other hand, the 4-bromo-2-fluorobenzyl group fitted into the hydrophobic cleft of AR, similar to the location of the benzothiazole ring of zopolrestat, so that each halogen atom was linked by a hydrogen bond to Leu300 backbone NH or to Thr113 Oγ1H. Other important features were van der Waals interactions; the aromatic side chains of Trp20 and Phe122 were positioned to sandwich the pyrrolopyrazine framework, and Trp111 and Leu300 intercalated the 4-bromo-2-fluorobenzyl group. Thus, the mode of binding of the *R*-isomer to AR is likely to resemble that of zopolrestat, and this makes the *R*-isomer a very potent inhibitor of AR.

Figure 11 displays the flexible docked structure of SX-3202 (*S*-isomer) superposed on that of AS-3201 (*R*-isomer) in the active site of AR. The similar molecular modeling experiments placed the *S*-isomer in an orientation different from that of the *R*-isomer, and the flexible docked complex was less stable than that for the *R*-isomer by approximately 17 kJ/mol. The accommodation of the succinimide ring of the *S*-isomer was better when the 5′-carbonyl oxygen made bifurcated hydrogen bonds to Tyr48 and His110. However, the 1′-nitrogen did not contribute to binding (1′-N to Tyr48 OηH, 3.2 Å), and the 2′-carbonyl oxygen pointed away from these active center residues and was oriented toward Trp20, forming a hydrogen bond to the unexpectedly flipped indole ring. In the allowed conformational state, the aromatic side chain of Phe122 as well as that of Trp20 was displaced through the van der Waals interactions with the pyrrolopyrazine framework, and Trp111 Nϵ1H was away from the succinimide and now near to the 3-carbonyl oxygen, which was still bound to Cys298 SγH. Also noteworthy was the fact that the relative orientation of the 4-bromo-2-fluorobenzyl group of the *S*-isomer was slightly different from that of the *R*-isomer. The 2-fluorine atom was placed outside the hydrogen bond contact with backbone NH of Leu300 (3.5 Å), whereas that in the *R*-isomer complex was within the hydrogen bond distance of this NH (2.5 Å). On the whole, the *S*-isomer at the active site was held in place by six hydrogen bonds whereas that of the *R*-isomer by eight.

DISCUSSION

Interruption of the polyol pathway with the use of ARIs has been extensively studied as a therapeutic strategy for preventing the onset or delaying the progression of diabetic complications. AS-3201 (*R*-isomer) is a structurally novel and highly potent ARI with improved pharmacokinetics (*16*). The focus of the present research was to describe the stereospecific and selective interaction in the binding site as well as to characterize the inhibition mechanism. The use of the low-affinity isomer (*S*-isomer) allowed us to examine the interaction with greater precision, and the comparative study of these E−I complexes provided meaningful information about the stereospecific interaction.

Inhibition Characteristics of the R- and S-Isomers. The inhibition of AR by the isomers was uncompetitive with respect to D-glucose in the forward reaction (aldehyde reduction), while in the reverse reaction (alcohol oxidation), their inhibition patterns were competitive with respect to D-sorbitol, irrespective of the difference in affinity for the enzyme. Since AR follows an ordered bi-bi mechanism where in the forward reaction the apoenzyme binds NADPH first and releases $NADP^+$ last, and vice versa in the reverse reaction (*11*−*13*), the results presented here support the idea that both isomers bind selectively to the E−$NADP^+$ binary complex during steady-state turnover. One explanation for these inhibition patterns assumes that the isomers strongly bind to the E−$NADP^+$ complex. Another may be ascribed to the fact that the E−$NADP^+$ complex is predominant during steady-state turnover. To clarify the characteristics of AR inhibition by the isomers, we examined complex formation between the isomers and each of the intermediate enzyme forms (the apoenzyme E and the E−$NADP^+$ and E−NADPH complexes).

The important feature for the present isomers is that the dissociation constant for dissociation of the *R*-isomer (or the *S*-isomer) from the E−$NADP^+$ complex (K_{dAB}) is almost the same as that for the E−NADPH complex (Table 4). Also, the presence of $NADP^+$ provided no synergetic protection against AR inactivation by NBS (Table 5). These results indicated that the presence of $NADP^+$ is not critical for the isomers binding to AR, and it is unlikely that the inhibition patterns concerning our isomers are attributable to the stronger binding to the E−$NADP^+$ complex, as demonstrated for a carboxylic acid type ARI, alrestatin (*45*). According to the transient kinetic analysis for partial reactions of AR, it was suggested that most of the enzyme is present as the E−$NADP^+$ complex during steady-state turnover (*12*, *46*). Therefore, the inhibition patterns are perhaps an expression of the kinetic specificity of the enzyme (the predominance of the E−$NADP^+$ complex) during steady-state turnover, rather than of binding specificity.

Binding Site of the R- and S-Isomers. The binding behavior of our isomers is distinct from that of some other ARIs; the isomers can bind to the apoenzyme as well as the holoenzyme, whereas sorbinil, alrestatin, and tolrestat do not (*45*, *47*, *48*). These findings led us to experimentally ascertain the binding site of the isomers as novel ARIs of spiro-succinimide type. Although a difference in the binding site of the isomers could be one of the causes of enantioselective inhibition, a ^{19}F NMR study revealed that the *R*- and *S*-isomers bind to the same site of AR. On the other hand, fluorescence methods showed that the dissociation constants (K_d) for dissociation of the isomers from the E−coenzyme complexes have finite and fixed values (Table 4), thus most simply indicating that the isomers bind at a site other than the coenzyme-binding site. Moreover, ponalrestat, an active site-directed ARI (*18*), and the *R*-isomer compete for the same binding site, or the binding of ponalrestat causes a conformational change in the enzyme molecule so as to prevent the subsequent binding of the *R*-isomer at a different site. This point was made clearer from the protective effect of the *S*-isomer on AR inactivation by NBS. The similarity in this effect between ponalrestat and the *S*-isomer clearly indicated that the *S*-isomer (and the *R*-isomer) binds to the active site of the enzyme as does ponalrestat, and further suggests that the formed E−I complexes might be conformationally similar despite the apparent difference in structure between ponalrestat and the isomers.

The pH-dependent feature of the inhibition provides another base for studying the inhibitor-binding site since it could result from changes in the ionization of the inhibitor, enzyme, or both. As mentioned in the preceding section, K_{ii} in the forward reaction is actually identical to the dissociation constant for dissociation of the isomers from the E−NADP$^+$ complex. Therefore, the pK_{ii}−pH profiles (Figure 4) show that the enzyme residue with a p*K* of 7.7−7.8 may be associated with the binding of the isomers and ponalrestat to the E−NADP$^+$ complex. This p*K* value was comparable to that reported for the active site catalytic residue (Tyr48, pK = 7.6) in the E−NADP$^+$ complex (*13*), consistent with all the results discussed above.

Forces Contributing to the Complex Formations and Binding Modes of the Isomers. Thus far, the stereospecificity of AR toward substrates or inhibitors has been investigated. However, little is known about the differences in the binding mode and/or conformation between these compounds. The use of our *R*- and *S*-isomers may serve as a probe for the stereospecificity because these isomers are conformationally restricted and active site-directed inhibitors (see above).

From the comparison of the thermodynamic parameter values, the difference in nature of E−I complex formation may be drawn between the isomers. The binding of the *S*-isomer is characterized by comparatively small negative enthalpy and large positive entropy changes whereas that of the *R*-isomer by the large negative enthalpy and small entropy changes. In other words, $\Delta H°$ and $\Delta S°$ for E−*R*-isomer complex formation are more negative than those for the E−*S*-isomer complex. Ross and Subramanian (*49*) suggested that protein−ligand association occurs in two steps: (step 1) hydrophobic association and partial immobilization, in which the release of water molecules that are restricted to the interacting hydrophobic surface is the source of significant positive entropy, and (step 2) formation of other intermolecular interactions, in which the strengthening of hydrogen bonds in the low-dielectric protein interior and van der Waals interactions are the most important factors contributing to the observed negative values of $\Delta H°$ and $\Delta S°$. The results given in Table 3 suggest that hydrophobic interaction (step 1) contributes significantly to E−*S*-isomer complex formation, and the conformational entropy losses upon complexation might be relatively small due to the rigidity of the isomer. In contrast, the more negative values of $\Delta H°$ and $\Delta S°$ for the E−*R*-isomer complex lead us to speculate that not hydrophobic interaction (step 1) but subsequent intermolecular interactions (step 2) such as hydrogen bonds and/or van der Waals interactions might account for the stronger binding of the *R*-isomer to the enzyme. Many of the antigen−antibody complexes belong to this "enthalpically driven" category (*50*, *51*), and this thermodynamic behavior has been attributed to these specific intermolecular interactions (*49*, *52*). It can be concluded, therefore, that the formation of additional hydrogen bonds and/or van der Waals interactions contributes to the energetic stabilization in the E−*R*-isomer complex.

Molecular modeling also shows that the binding mode of the *R*-isomer is different from that of the *S*-isomer. In the E−*R*-isomer complex, the succinimide ring is favorably located so that the heteroatoms form hydrogen bonds to the side chains of active site residues (Tyr48, His110, and Trp111), and the pyrrolopyrazine framework was firmly anchored to the active site through this hydrogen-bonding network and van der Waals interactions with Trp20 and Phe122. In contrast, the heteroatoms of the succinimide ring of the *S*-isomer do not form such a tight hydrogen-bonding network with the enzyme due to less matching to these active site residues (Figure 11). Moreover, the displacements of Trp20 and Trp111 in the E−*S*-isomer complex may perturb the van der Waals interactions so as to lower binding affinity, because these residues play important roles in inhibitor binding to AR (*45*, *53*, *54*). This modification in the interaction with Trp residues is consistent with the greater Stokes shift (the less blue shift) in the fluorescence spectra of the E−*S*-isomer complex as shown in Figure 6.

Furthermore, the ^{19}F NMR spectra have revealed that the local environment of the 2-fluorine atom in the E−*R*-isomer complex is different from that in the E−*S*-isomer complex. The two major determinants of fluorine chemical shifts are likely to be van der Waals interactions, which usually produce downfield shifts, and the magnetic anisotropy effects from aromatic rings, carbonyls, and other anisotropic groups, which at best produce either upfield or downfield shifts of $\pm$2 ppm (*55*−*57*). Since observation of an upfield fluorine shift is indicative of magnetic anisotropy effects from aromatic rings (ring current effect) on the bound fluorine (*56*), the upfield shift of the *R*-isomer signal on binding (0.79 ppm) suggests a substantial contribution from the ring current effect. In the E−*R*-isomer complex model, the 4-bromo-2-fluorobenzyl group is in a close stacking orientation with the indole ring of Trp111, and the 2-fluorine atom makes a hydrogen bond to Leu300 backbone NH. These interactions are absent from the E−*S*-isomer complex model (Figure 11). Also, the signals of the bound and free *R*-isomer are in slow exchange on the NMR time scale, whereas those of the bound and free *S*-isomer are in slow to intermediate exchange, indicating that AR binds the pendent benzyl group of the *R*-isomer more tightly than that of the *S*-isomer. Although the contribution of hydrogen bonding to fluorine shifts is uncertain (*56*), Negoro et al. (*16*) pointed out that the introduction of a fluorine atom at position C-2 of the pendent benzyl group results in a significant improvement in AR inhibitory activity. Therefore, it can be reasoned that the hydrogen-bonding interaction of the fluorine atom with Leu300 backbone NH as well as the van der Waals interactions of the 4-bromo-2-fluorobenzyl group with the indole ring of Trp111 may enhance the stereospecificity of AR toward the isomers.

According to the structure-based thermodynamic analysis, most of the enthalpically favorable interactions for the E−*R*-isomer complex are due to these specific hydrogen-bonding and van der Waals interactions described above. These interactions may be further strengthened in the low-dielectric interacting surface, which is presumed upon the blue shift in the emission maximum of the complex (Figure 6). Since each hydrogen bond effects a binding strength by approximately 7−10 kJ/mol (*58*−*60*), the view that eventually two additional hydrogen bonds are present between the *R*-isomer and AR is in fairly good agreement with the difference in binding energy between the present isomer complexes (Table 3).

Selectivity of the Isomers between AR and ALR. It is generally believed that one cause of clinical side effects of ARIs is related to nonselective inhibition of aldehyde reductase (ALR), a closely related enzyme, and the participation of nonconserved active site residues in the binding of inhibitors is responsible for the differences in the potency of inhibition of AR and ALR (*61*). Since the tertiary structures of porcine ALR and human AR can be superposed upon each other in the active site except for residues 300−305 near the C-terminal end (*62*), it should be noted that Leu300 in AR is changed to Pro in ALR, which would not have the ability to form a hydrogen bond to the 2-fluorine atom of the pendent benzyl ring. To make this point clearer, we examined the *R*- and *S*-isomers for ALR inhibitory activity by using ALR purified from porcine kidney. The kinetic study demonstrated that the inhibitor constant of the *R*-isomer was 3×10^{-7} M while that of the *S*-isomer was 7×10^{-7} M in porcine kidney ALR (unpublished data), indicating that the failure of the 2-fluorine atom to form a hydrogen bond with ALR accounts for such a decrease in stereospecificity.[10] This result supports the idea that the formation of an additional hydrogen bond between the pendent benzyl ring of the *R*-isomer and AR leads to the differentiation between AR and ALR as well as the thermodynamic stabilization of the E−*R*-isomer complex.

In summary, we have characterized the interaction of AS-3201 (*R*-isomer) with AR, in comparison with that of the optical isomer (*S*-isomer). Although the difference in stereostructure in the succinimide ring induced an ∼2000-fold change in the inhibitor constant (K_i), both isomers are active site-directed inhibitors, which seem to preferentially bind to the E−NADP$^+$ complex during the steady-state turnover. Molecular modeling, together with the deductions from spectroscopic studies, suggested that the succinimide ring in the *R*-configuration binds more optimally in the enzyme active site to form a hydrogen-bonding network and the 2-fluorine atom of the pendent benzyl group may interact with AR by forming an additional hydrogen bond to one of the residues that are not conserved in ALR (a closely related enzyme). Thus, the results presented here reinforce the view that the *R*-isomer acts as a stereospecifically potent and selective ARI.

[10] The results showed that the ratio of K_i(porcine ALR) to K_i(human AR) for the *R*-isomer is more than 800 while that for the *S*-isomer is ∼1. Since a high degree of sequence homology exists between porcine ALR and human ALR (*62*), the ratio of K_i(human ALR) to K_i(human AR) for the *R*-isomer, i.e., the selectivity of the *R*-isomer against the human enzymes, is also inferred to be high.

ACKNOWLEDGMENT

We are grateful to Mr. T. Ueda for NMR measurements, to Mr. Y. Ono and Mr. K. Nakamura for porcine ALR purification, and to Drs. M. Komiya and J. Kuwasima for helpful discussions on several points in the paper. We also thank Dr. T. Karasawa, the director of this laboratory, for his continuing interest and encouragement.

REFERENCES

1. Hers, H. G. (1956) *Biochim. Biophys. Acta 22*, 202−203.
2. Van Heyningen, R. (1959) *Nature 184*, 194−195.
3. Kador, P. F. (1988) *Med. Res. Rev. 8*, 325−352.
4. Kinoshita, J. H., and Nishimura, C. (1988) *Diabetes Metab. Rev. 4*, 323−337.
5. Tilton, R. G., Chang, K., Hasan, K. S., Smith, S. R., Petrash, J. M., Misko, T. P., Moore, W. M., Currie, M. G., Corbett, J. A., McDaniel, M. L., and Williamson, J. R. (1993) *Diabetes 42*, 221−232.
6. Kador, P. F., Akagi, Y., Takahashi, Y., Ikebe, H., Wyman, M., and Kinoshita, J. H. (1990) *Arch. Ophthalmol. 108*, 1301−1309.
7. Engerman, R. L., and Kern, T. S. (1993) *Diabetes 42*, 820−825.
8. Cameron, N. E., and Cotter, M. A. (1992) *Br. J. Pharmacol. 107*, 939−944.
9. Frank, R. N. (1994) *Diabetes 43*, 169−172.
10. Pfeifer, M. A., Schumer, M. P., and Gelber, D. A. (1997) *Diabetes 46*, S82−S89.
11. Kubiseski, T. J., Hyndman, D. J., Morjana, N. A., and Flynn, T. G. (1992) *J. Biol. Chem. 267*, 6510−6517.
12. Grimshaw, C. E., Bohren, K. M., Lai, C.-J., and Gabbay, K. H. (1995) *Biochemistry 34*, 14356−14365.
13. Grimshaw, C. E., Bohren, K. M., Lai, C.-J., and Gabbay, K. H. (1995) *Biochemistry 34*, 14374−14384.
14. Tarle, I., Borhani, D. W., Wilson, D. K., Quiocho, F. A., and Petrash, J. M. (1993) *J. Biol. Chem. 268*, 25687−25693.
15. Bohren, K. M., Grimshaw, C. E., Lai, C.-J., Harrison, D. H., Ringe, D., Petsko, G. A., and Gabbay, K. H. (1994) *Biochemistry 33*, 2021−2032.
16. Negoro, T., Murata, M., Ueda, S., Fujitani, B., Ono, Y., Kuromiya, A., Komiya, M., Suzuki, K., and Matsumoto, J. (1998) *J. Med. Chem. 41*, 4118−4129.
17. Nishimura, C., Yamaoka, T., Mizutani, M., Yamashita, K., Akera, T., and Tanimoto, T. (1991) *Biochim. Biophys. Acta 1078*, 171−178.
18. Lee, Y. S., Chen, Z., and Kador, P. F. (1998) *Bioorg. Med. Chem. 6*, 1811−1819.
19. Wilson, D. K., Tarle, I., Petrash, J. M., and Quiocho, F. A. (1993) *Proc. Natl. Acad. Sci. U.S.A. 90*, 9847−9851.
20. Cleland, W. W. (1979) *Methods Enzymol. 63*, 500−513.
21. Duggleby, R. G. (1988) *Biochem. Med. Metab. Biol. 40*, 204−212.
22. Brandt, R. B., Laux, J. E., and Yates, S. W. (1987) *Biochem. Med. Metab. Biol. 37*, 344−349.
23. Williams, E. A., and Morrison, J. F. (1992) *Biochemistry 31*, 6801−6811.
24. Henderson, P. J. F. (1972) *Biochem. J. 127*, 321−333.
25. Cha, S. (1975) *Biochem. Pharmacol. 24*, 2177−2185.
26. Cleland, W. W. (1963) *Biochim. Biophys. Acta 67*, 173−187.
27. Williams, J. W., and Morrison, J. F. (1979) *Methods Enzymol. 63*, 437−467.
28. Dunn, S. M. J., Batchelor, J. G., and King, R. W. (1978) *Biochemistry 17*, 2356−2364.

29. Birdsall, B., Burgen, A. S. V., Rodrigues de Miranda, J., and Roberts, G. C. K. (1978) *Biochemistry 17*, 2102−2110.
30. Wilson, D. K., Bohren, K. M., Gabbay, K. H., and Quiocho, F. A. (1992) *Science 257*, 81−84.
31. Weiner, S. J., Kollman, P. A., Nguyen, D. T., and Case, D. A. (1986) *J. Comput. Chem. 7*, 230−252.
32. Greengard, L., and Rokhlin, V. I. (1987) *J. Comput. Phys. 73*, 325.
33. Hagler, A. T., Osguthorpe, D. J., Dauber-Osguthorpe, P., and Hempel, J. C. (1985) *Science 227*, 1309−1315.
34. Clark, M., Cramer, R. D., III, and Van Opdenbosch, N. (1989) *J. Comput. Chem. 10*, 982−1012.
35. Dixon, M., and Webb, E. C. (1979) in *Enzymes*, 3rd ed., pp 337−338, Longman Group Ltd., London.
36. Laskowski, M., Jr., and Sealock, R. W. (1971) in *The Enzymes* (Boyer, P. D., Ed.) Vol. III, pp 391−393, Academic Press, New York.
37. Bhatnagar, A., Liu, S.-Q., Ueno, N., Chakrabarti, B., and Srivastava, S. K. (1994) *Biochim. Biophys. Acta 1205*, 207−214.
38. Brittain, D. R. (1986) *Spec. Publ.*−*R. Soc. Chem. 55*, 210−240.
39. vander Jagt, D. L., Kolb, N. S., vander Jagt, T. J., Chino, J., Martinez, F. J., Hunsaker, L. A., and Royer, R. E. (1995) *Biochim. Biophys. Acta 1249*, 117−126.
40. Kubiseski, T. J., and Flynn, T. G. (1995) *J. Biol. Chem. 270*, 16911−16917.
41. Spande, T. F., and Witkop, B. (1967) *Methods Enzymol. 11*, 498−506.
42. Ohnishi, M., Kawagishi, T., Abe, T., and Hiromi, K. (1980) *J. Biochem. 87*, 273−279.
43. Urzhumtsev, A., Tete-Favier, F., Mitschler, A., Barbanton, J., Barth, P., Urzhumtseva, L., Biellmann, J. F., Podjarny, A., and Moras, D. (1997) *Structure 5*, 601−612.
44. Oka, M., Matsumoto, Y., Sugiyama, S., Tsuruta, N., and Matsushima, M. (2000) *J. Med. Chem. 43*, 2479−2483.
45. Ehrig, T., Bohren, K. M., Prendergast, F. G., and Gabby, K. H. (1994) *Biochemistry 33*, 7157−7165.
46. Grimshaw, C. E., and Lai, C.-J. (1995) *Adv. Exp. Med. Biol. 372*, 229−240.
47. Nakano, T., and Petrash, J. M. (1996) *Biochemistry 35*, 11196−11202.
48. Sugiyama, K., Chen, Z., Lee, Y. S., and Kador, P. F. (2000) *Biochem. Pharmacol. 59*, 329−336.
49. Ross, P. D., and Subramanian, S. (1981) *Biochemistry 20*, 3096−3102.
50. Hibbits, K. A., Gill, D. S., and Willson, R. C. (1994) *Biochemistry 33*, 3584−3590.
51. Tello, D., Goldbaum, F. A., Mariuzza, R. A., Ysern, X., Schwarz, F. P., and Poljak, R. J. (1993) *Biochem. Soc. Trans. 21*, 943−946.
52. Sturtevant, J. M. (1977) *Proc. Natl. Acad. Sci. U.S.A. 74*, 2236−2240.
53. Hohman, T. C., El-Kabbani, O., Malamas, M. S., Lai, K., Putilina, T., McGowan, M. H., Wane, Y. Q., and Carper, D. A. (1998) *Eur. J. Biochem. 256*, 310−316.
54. Singh, S. B., Malamas, M. S., Hohman, T. C., Nilakantan, R., Carper, D. A., and Kitchen, D. (2000) *J. Med. Chem. 43*, 1062−1070.
55. Hull, W. E., and Sykes, B. D. (1976) *Biochemistry 15*, 1535−1546.
56. Gregory, D. H., and Gerig, J. T. (1991) *Biopolymers 31*, 845−858.
57. Chambers, S. E., Lau, E. Y., and Gerig, J. T. (1994) *J. Am. Chem. Soc. 116*, 3603−3604.
58. Privalov, P. L., and Makhatadze, G. I. (1993) *J. Mol. Biol. 232*, 660−679.
59. Yamagata, Y., Kubota, M., Sumikawa, Y., Funahashi, J., Takano, K., Fujii, S., and Yutani, K. (1998) *Biochemistry 37*, 9355−9362.
60. Takano, K., Yamagata, Y., Kubota, M., Funahashi, J., Fujii, S., and Yutani, K. (1999) *Biochemistry 38*, 6623−6629.
61. Jez, J. M., Bennett, M. J., Schlegel, B. P., Lewis, M., and Penning, T. M. (1997) *Biochem. J. 326*, 625−636.
62. El-Kabbani, O., Judge, K., Ginell, S. L., Myles, D. A., DeLucas, L. J., and Flynn, T. G. (1995) *Nat. Struct. Biol. 2*, 687−692.

BI0102813